

DARL1N: Distributed multi-Agent Reinforcement Learning with One-hop Neighbors

Baoqian Wang^{1,2}, Junfei Xie² and Nikolay Atanasov¹

¹University of California, San Diego

²San Diego State University

bawang@ucsd.edu, jxie4@sdsu.edu, natanasov@ucsd.edu

Abstract

Most existing multi-agent reinforcement learning (MARL) methods are limited in the scale of problems they can handle. Particularly, with the increase of the number of agents, their training costs grow exponentially. In this paper, we address this limitation by introducing a scalable MARL method called Distributed multi-Agent Reinforcement Learning with One-hop Neighbors (DARL1N). DARL1N is an off-policy actor-critic method that breaks the curse of dimensionality by decoupling the global interactions among agents and restricting information exchanges to one-hop neighbors. Each agent optimizes its action value and policy functions over a one-hop neighborhood, significantly reducing the learning complexity, yet maintaining expressiveness by training with varying numbers and states of neighbors. This structure allows us to formulate a distributed learning framework to further speed up the training procedure. Comparisons with state-of-the-art MARL methods show that DARL1N significantly reduces training time without sacrificing policy quality and is scalable as the number of agents increases.

1 Introduction

Recent years have witnessed tremendous success of reinforcement learning (RL) in challenging decision making problems, such as robot control and video games. Research efforts are currently focused on multi-agent settings, such as cooperative robot navigation, multi-player games, and traffic management. A direct application of RL techniques in a multi-agent setting by simultaneously running a single-agent algorithm on each agent exhibits poor performance [Lowe *et al.*, 2017]. This is because, without considering interactions among the agents, the environment becomes non-stationary from the perspective of a single agent.

Multi-agent reinforcement learning (MARL) [Buşoniu *et al.*, 2010] addresses the aforementioned challenge by considering all agents and their dynamics collectively when learning the policy of an individual agent. This is achieved by learning a centralized value or action-value (Q) function that involves the states and actions of all agents. Most effective MARL algorithms, such as multi-agent deep deterministic

policy gradient (MADDPG) [Lowe *et al.*, 2017], counterfactual multi-agent (COMA) [Foerster *et al.*, 2018], and multi actor attention critic (MAAC) [Iqbal and Sha, 2019], adopt this strategy. However, learning a centralized value/Q function is challenging due to the exponentially growing joint state and action spaces with the increasing number of agents [Qu *et al.*, 2020]. The trained policies have poor performance in large-scale settings as shown in [Yang *et al.*, 2018; Long *et al.*, 2020].

Recently, MARL algorithms that significantly improve the quality of learned policies for large-scale multi-agent settings were proposed such as the value factorization based algorithms (e.g., mean-field MARL [Yang *et al.*, 2018]), evolutionary population curriculum (EPC) [Long *et al.*, 2020] and scalable actor critic (SAC) [Qu *et al.*, 2020]. While these methods achieve excellent performance, their training costs are still very large as the number of agents increases, because they cannot be easily trained in a fully distributed manner.

Our **contribution** is a scalable and efficient MARL method called Distributed multi-Agent Reinforcement Learning with One-hop Neighbors (DARL1N). Its main advantage over state-of-the-art methods is a distributed training framework, in which each compute node only simulates a very small subset of the agents. This is made possible by representing the agent topology as a disk proximity graph and approximating the Q function over one-hop neighborhoods. When agent interactions are restricted to one-hop neighbors, training the Q function of an agent requires simulation only of the agent itself and its potential two-hop neighbors. This enables highly efficient distributed training and greatly accelerates the training speed of large-scale multi-agent policies.

2 Related Work

2.1 Multi-Agent Reinforcement Learning

Typical MARL algorithms like MADDPG [Lowe *et al.*, 2017], COMA [Foerster *et al.*, 2018], and MAAC [Iqbal and Sha, 2019] require learning a centralized value/Q function. They achieve effective performance but cannot scale to large numbers of agents. The exponentially growing joint state and action spaces make learning accurate value/Q functions increasingly challenging. This issue can be alleviated by factorizing the value/Q function into a combination of independent utility functions that only depend on the local observations

and actions of each agent. For example, in VDN [Sunehag *et al.*, 2017], the utility functions are added up to construct the Q function, but full factorization with simple summing limits the type of Q functions that can be learned. QMIX [Rashid *et al.*, 2018] improves VDN by combining the utility functions monotonically using a mixing neural network, which makes it applicable for more general Q functions. QTRAN [Son *et al.*, 2019] further extends VDN and QMIX to more general MARL settings by factorizing a transforming value function without additivity and monotonicity assumptions.

The value/Q function can also be factorized according to a coordination graph. For instance, [Kuyer *et al.*, 2008] decomposed the Q function into a set of payoff functions with pairwise dependencies specified by agents that are connected in an undirected graph. [Böhmer *et al.*, 2020] factorized the Q function into both utility and payoff functions according to a coordination graph learned by a deep neural network. Mean-Field MARL [Yang *et al.*, 2018] including Mean-Field Actor Critic (MFAC) and Mean-Field Q (MF-Q) further approximate the factorized Q function according to the macro behavior of the agents.

In addition to value factorization, there are a few other methods proposed to enable scalable MARL. EPC [Long *et al.*, 2020] applies curriculum learning to gradually scale MARL up. It adopts population invariant policy and Q functions to support variant numbers of agents in different learning stages. To further speed up training, this method is implemented in a parallel computing architecture that consists of multiple compute nodes, each running multiple processes. In each compute node, agents are trained in multiple independent environments in parallel, and each environment and agent run in a separate process. Another method closely related to this paper is SAC [Qu *et al.*, 2020], which approximates the Q function of each agent using the states and actions of its κ -hop neighbors. The idea is similar to ours but training SAC is costly and cannot be distributed, as it uses gradient descent with momentum for learning the Q function, which requires simultaneous simulation of multi-step transitions for many agents.

2.2 Distributed and Parallel Architectures for RL

Multiple distributed or parallel architectures have been proposed to accelerate RL training. The first massive parallel architecture was presented in [Nair *et al.*, 2015] to train deep Q networks. It creates multiple actors and learners, with each actor interacting with its environment independently and each learner updating the parameters. This architecture, however, only works for off-policy RL algorithms. To support both off-policy and on-policy RL algorithms, a more general parallel architecture called A3C [Mnih *et al.*, 2016] was then developed, as well as its multiple variants, such as the A2C [OpenAI, 2022] and GA3C [Babaeizadeh *et al.*, 2017]. The A3C has also been extended to multi-agent settings [Simões *et al.*, 2020], where each computing instance performs an independent training for all agent parameters asynchronously. Also of interest is the distributed architecture presented in [Chen *et al.*, 2018], which was designed to reduce the communication overhead between learners and the central controller. Although these methods can reduce the training time by dis-

tributing the computation load, they cannot reduce the total computation load, and hence their training costs are still high.

3 Background

This section introduces the MARL problem. In MARL, M agents learn to optimize their behaviors by interacting with the environment. Denote the state and action of agent $i \in [M] := \{1, \dots, M\}$ by $s_i \in \mathcal{S}_i$ and $a_i \in \mathcal{A}_i$, respectively, where \mathcal{S}_i and \mathcal{A}_i are the corresponding state and action spaces. Let $\mathbf{s} := (s_1, \dots, s_M) \in \mathcal{S} := \prod_{i \in [M]} \mathcal{S}_i$ and $\mathbf{a} := (a_1, \dots, a_M) \in \mathcal{A} := \prod_{i \in [M]} \mathcal{A}_i$ denote the joint state and action of all agents. At time t , a joint action $\mathbf{a}(t)$ applied at state $\mathbf{s}(t)$ triggers a transition to a new state $\mathbf{s}(t+1) \in \mathcal{S}$ according to a conditional probability density function (pdf) $p(\mathbf{s}(t+1)|\mathbf{s}(t), \mathbf{a}(t))$. After each transition, each agent i receives a reward $r_i(\mathbf{s}(t), \mathbf{a}(t))$, determined by the joint state and action according to the function $r_i : \mathcal{S} \times \mathcal{A} \mapsto \mathbb{R}$.

The objective of each agent i is to choose a policy $\mu_i : \mathcal{S} \rightarrow \mathcal{A}_i$ to maximize the expected cumulative discounted reward:

$$V_i^\mu(\mathbf{s}) := \mathbb{E}_{\substack{\mathbf{a}(t)=\mu(\mathbf{s}(t)) \\ \mathbf{s}(t) \sim p}} \left[\sum_{t=0}^{\infty} \gamma^t r_i(\mathbf{s}(t), \mathbf{a}(t)) \mid \mathbf{s}(0) = \mathbf{s} \right],$$

where $\mu := (\mu_1, \dots, \mu_M)$ denotes the joint policy of all agents and $\gamma \in (0, 1)$ is a discount factor. The function $V_i^\mu(\mathbf{s})$ is known as the *value function* of agent i associated with joint policy μ . Many RL and MARL techniques consider stochastic policies to support the exploration-exploitation trade-off when approximating the value and policy functions [Sutton and Barto, 2018]. However, since optimal policies are known to be deterministic, it is possible to directly restrict attention to deterministic policies during the learning process, e.g., as done in DDPG [Lillicrap *et al.*, 2016] and MADDPG [Lowe *et al.*, 2017].

An optimal policy μ_i^* for agent i can also be obtained by maximizing the *action-value (Q) function*:

$$Q_i^\mu(\mathbf{s}, \mathbf{a}) := \mathbb{E}_{\substack{\mathbf{a}(t)=\mu(\mathbf{s}(t)) \\ \mathbf{s}(t) \sim p}} \left[\sum_{t=0}^{\infty} \gamma^t r_i(\mathbf{s}(t), \mathbf{a}(t)) \mid \mathbf{s}(0) = \mathbf{s}, \mathbf{a}(0) = \mathbf{a} \right]$$

and setting $\mu_i^*(\mathbf{s}) \in \arg \max_{a_i} \max_{\mathbf{a}_{-i}} Q_i^*(\mathbf{s}, \mathbf{a})$, where $Q_i^*(\mathbf{s}, \mathbf{a}) := \max_{\mu} Q_i^\mu(\mathbf{s}, \mathbf{a})$ and \mathbf{a}_{-i} denotes the actions of all agents except i . In the rest of the paper, we omit the time notation t for simplicity, when there is no risk of confusion.

4 Problem Statement

To develop a distributed MARL algorithm, we impose additional structure on the MARL problem. Assume that all agents share a common state space, i.e., $\mathcal{S}_i = \mathcal{S}_j, \forall i, j \in [M]$. Let $dist : \mathcal{S}_i \times \mathcal{S}_i \rightarrow \mathbb{R}$ be a distance metric on the homogeneous state space. We introduce a proximity graph [Bullo *et al.*, 2009] to model the topology of the agent team. A d -disk proximity graph is defined as a mapping that associates the joint state $\mathbf{s} \in \mathcal{S}$ with an undirected graph $(\mathcal{V}, \mathcal{E})$ such that $\mathcal{V} = \{s_1, s_2, \dots, s_M\}$ and $\mathcal{E} = \{(s_i, s_j) | dist(s_i, s_j) \leq d, i \neq j\}$. Define the set of *one-hop neighbors* of agent i as $\mathcal{N}_i := \{j | (s_i, s_j) \in \mathcal{E}\} \cup \{i\}$. We make the following regularity assumption about the agents' motion.

Assumption 1. The distance between two consecutive states, $s_i(t)$ and $s_i(t+1)$, of agent i is bounded, i.e., $\text{dist}(s_i(t), s_i(t+1)) \leq \epsilon$, for some $\epsilon > 0$.

This assumption is justified in many problems of interest where, e.g., due to physical limitations, the agent states can only change by a bounded amount in a single time step. Following this assumption, we define the set of *potential neighbors* of agent i at time t as $\mathcal{P}_i(t) := \{j | \text{dist}(s_j(t), s_i(t)) \leq 2\epsilon + d\}$, which captures the set of agents that may become one-hop neighbors of agent i at time $t+1$.

Denote the joint state and action of the one-hop neighbors of agent i by $\mathbf{s}_{\mathcal{N}_i} = (s_{j_1}, \dots, s_{j_{|\mathcal{N}_i|}})$ and $\mathbf{a}_{\mathcal{N}_i} = (a_{j_1}, \dots, a_{j_{|\mathcal{N}_i|}})$, respectively, where $j_1, \dots, j_{|\mathcal{N}_i|} \in \mathcal{N}_i$. Our key idea is to let agent i 's policy, $a_i = \mu_i(\mathbf{s}_{\mathcal{N}_i})$, only depend on the one-hop neighbor states $\mathbf{s}_{\mathcal{N}_i}$. The intuition is that agents that are far away from agent i at time t have little impact on its current action $a_i(t)$. To support this policy model, we make two additional assumptions on the problem structure. To emphasize that the output of a function $f : \prod_{i \in [M]} \mathcal{S}_i \mapsto \mathbb{R}$ is affected only by a subset $\mathcal{N} \subseteq [M]$ of the input dimensions, we use the notation $f(\mathbf{s}) = f(\mathbf{s}_{\mathcal{N}})$ for $\mathbf{s} \in \mathcal{S}$ and $\mathbf{s}_{\mathcal{N}} \in \prod_{i \in \mathcal{N}} \mathcal{S}_i$.

Assumption 2. The reward of agent i can be fully specified using its one-hop neighbor states $\mathbf{s}_{\mathcal{N}_i}$ and actions $\mathbf{a}_{\mathcal{N}_i}$, i.e., $r_i(\mathbf{s}, \mathbf{a}) = r_i(\mathbf{s}_{\mathcal{N}_i}, \mathbf{a}_{\mathcal{N}_i})$ and its absolute value is upper bounded by $|r_i(\mathbf{s}_{\mathcal{N}_i}, \mathbf{a}_{\mathcal{N}_i})| \leq \bar{r}$, for some $\bar{r} > 0$.

Assumption 2 is satisfied in many multi-agent problems where the reward of one agent is determined only by the states and actions of nearby agents. Examples are provided in Sec. 6. Similar assumptions are adopted in [Qu *et al.*, 2020; Chu *et al.*, 2019; Lin *et al.*, 2020].

Assumption 3. The transition model of agent i depends only on its action a_i and one-hop neighbor states $\mathbf{s}_{\mathcal{N}_i}$, i.e., $p_i(s_i(t+1) | \mathbf{s}(t), a_i(t)) = p_i(s_i(t+1) | \mathbf{s}_{\mathcal{N}_i}(t), a_i(t))$.

Assumption 3 is common for multi-agent networked systems as in [Qu *et al.*, 2020; Lin *et al.*, 2020]. As a result, the joint state transition pdf decomposes as:

$$p(\mathbf{s}(t+1) | \mathbf{s}(t), \mathbf{a}(t)) = \prod_{i=1}^M p_i(s_i(t+1) | \mathbf{s}_{\mathcal{N}_i}(t), a_i(t)).$$

The objective of each agent i is to obtain an optimal policy μ_i^* by solving the following problem:

$$\mu_i^*(\mathbf{s}_{\mathcal{N}_i}) = \arg \max_{a_i} \max_{\mathbf{a}_{-i}} Q_i^*(\mathbf{s}, \mathbf{a}),$$

where $Q_i^*(\mathbf{s}, \mathbf{a}) := \max_{\mu} Q_i^{\mu}(\mathbf{s}, \mathbf{a})$ is the optimal action-value (Q) function introduced in the previous section.

5 Methods

In this section, we develop the DARN1N algorithm to solve the MARL problem with proximity-graph structure. DARN1N limits the interactions among agents within one-hop neighbors to significantly reduce the learning complexity. To further speed training up, DARN1N adopts a distributed training framework that exploits local interactions to decompose and distribute the computation load.

5.1 One-hop Neighbor-based Learning

The Q function of each agent associated with the MARL problem over the proximity graph can be written as

$$Q_i^{\mu}(\mathbf{s}, \mathbf{a}) = Q_i^{\mu}(\mathbf{s}_{\mathcal{N}_i}, \mathbf{s}_{\mathcal{N}_i^-}, \mathbf{a}_{\mathcal{N}_i}, \mathbf{a}_{\mathcal{N}_i^-})$$

where $\mathbf{s}_{\mathcal{N}_i^-}, \mathbf{a}_{\mathcal{N}_i^-}$ denote joint states and actions of agents except one-hop neighbors of agent i . Inspired by the SAC algorithm [Qu *et al.*, 2020], we approximate the Q function as \tilde{Q}_i^{μ} that depends only on one-hop neighbor states and actions:

$$\begin{aligned} \tilde{Q}_i^{\mu}(\mathbf{s}_{\mathcal{N}_i}, \mathbf{a}_{\mathcal{N}_i}) &= \sum_{\mathbf{s}_{\mathcal{N}_i^-}, \mathbf{a}_{\mathcal{N}_i^-}} w_i(\mathbf{s}_{\mathcal{N}_i}, \mathbf{s}_{\mathcal{N}_i^-}, \mathbf{a}_{\mathcal{N}_i}, \mathbf{a}_{\mathcal{N}_i^-}) Q_i^{\mu}(\mathbf{s}_{\mathcal{N}_i}, \mathbf{s}_{\mathcal{N}_i^-}, \mathbf{a}_{\mathcal{N}_i}, \mathbf{a}_{\mathcal{N}_i^-}) \end{aligned}$$

where the weights $w_i(\mathbf{s}_{\mathcal{N}_i}, \mathbf{s}_{\mathcal{N}_i^-}, \mathbf{a}_{\mathcal{N}_i}, \mathbf{a}_{\mathcal{N}_i^-}) > 0$ satisfy $\sum_{\mathbf{s}_{\mathcal{N}_i^-}, \mathbf{a}_{\mathcal{N}_i^-}} w_i(\mathbf{s}_{\mathcal{N}_i}, \mathbf{s}_{\mathcal{N}_i^-}, \mathbf{a}_{\mathcal{N}_i}, \mathbf{a}_{\mathcal{N}_i^-}) = 1$. The approximation error is given in the following lemma with proof provided in Appendix A.1.

Lemma 1. Under Assumptions 2 and 3, the approximation error between $\tilde{Q}_i^{\mu}(\mathbf{s}_{\mathcal{N}_i}, \mathbf{a}_{\mathcal{N}_i})$ and $Q_i^{\mu}(\mathbf{s}, \mathbf{a})$ is bounded by:

$$|\tilde{Q}_i^{\mu}(\mathbf{s}_{\mathcal{N}_i}, \mathbf{a}_{\mathcal{N}_i}) - Q_i^{\mu}(\mathbf{s}, \mathbf{a})| \leq \frac{2\bar{r}\gamma}{1-\gamma}.$$

It is worth noting that DARN1N uses a more general reward model $r_i(\mathbf{s}_{\mathcal{N}_i}, \mathbf{a}_{\mathcal{N}_i})$ compared to the model $r_i(s_i, a_i)$ used in SAC [Qu *et al.*, 2020].

We then parameterize the approximated Q function $\tilde{Q}_i^{\mu}(\mathbf{s}_{\mathcal{N}_i}, \mathbf{a}_{\mathcal{N}_i})$ and the policy $\mu_i(\mathbf{s}_{\mathcal{N}_i})$ by θ_i and ϕ_i , respectively. To handle the varying sizes of $\mathbf{s}_{\mathcal{N}_i}$ and $\mathbf{a}_{\mathcal{N}_i}$, in the implementation, we let the input dimension of \tilde{Q}_i^{μ} to be the largest possible dimension of $(\mathbf{s}_{\mathcal{N}_i}, \mathbf{a}_{\mathcal{N}_i})$, and apply zero-padding for agents that are not in the one-hop neighborhood of agent i . The same procedure is applied to represent $\mu_i(\mathbf{s}_{\mathcal{N}_i})$. More implementation details are provided in Appendix A.4.

To learn the approximated Q function \tilde{Q}_i^{μ} , instead of incremental on-policy updates to the Q function as in SAC, we adopt off-policy temporal-difference learning with a buffer similar to MADDPG. The parameters θ_i of the approximated Q function are updated by minimizing:

$$\begin{aligned} \mathcal{L}(\theta_i) &= \mathbb{E}_{(\mathbf{s}_{\mathcal{N}_i}, \mathbf{a}_{\mathcal{N}_i}, r_i, \{\mathbf{s}_{\mathcal{N}'_j}\}_{\forall j \in \mathcal{N}'_i}) \sim \mathcal{D}_i} \left[\left(\tilde{Q}_i^{\mu}(\mathbf{s}_{\mathcal{N}_i}, \mathbf{a}_{\mathcal{N}_i}) - y \right)^2 \right] \\ y &= r_i + \gamma \hat{Q}_i^{\hat{\mu}}(\mathbf{s}_{\mathcal{N}'_i}, \mathbf{a}_{\mathcal{N}'_i}) \end{aligned} \quad (1)$$

where \mathcal{D}_i is the replay buffer for agent i that contains information only from $\mathcal{N}_i, \mathcal{N}'_i$, the one-hop neighbors of agent i at the current and next time step, and the one-hop neighbors \mathcal{N}'_j for $j \in \mathcal{N}'_i$. To stabilize the training, a target Q function $\hat{Q}_i^{\hat{\mu}}$ with parameters $\hat{\theta}_i$ and a target policy function $\hat{\mu}_i$ with parameters $\hat{\phi}_i$ are used. The parameters $\hat{\theta}_i$ and $\hat{\phi}_i$ are updated using Polyak averaging, $\hat{\theta}_i = \tau \hat{\theta}_i + (1-\tau)\theta_i$ and $\hat{\phi}_i = \tau \hat{\phi}_i + (1-\tau)\phi_i$, where τ is a hyperparameter. In contrast to MADDPG, the replay buffer \mathcal{D}_i for agent i only needs to store its local interactions $(\mathbf{s}_{\mathcal{N}_i}, \mathbf{a}_{\mathcal{N}_i}, r_i, \{\mathbf{s}_{\mathcal{N}'_j}\}_{\forall j \in \mathcal{N}'_i})$ with nearby agents. Note that $\{\mathbf{s}_{\mathcal{N}'_j}\}_{\forall j \in \mathcal{N}'_i}$ is used to calculate $\mathbf{a}_{\mathcal{N}'_i}$.

Also, in contrast to SAC, each agent i only needs to collect its own training data by simulating local two-hop interactions. This allows an efficient and distributed training framework as we explain in the next subsection.

Agent i 's policy parameters ϕ_i are updated using gradients from the policy gradient theorem [Sutton and Barto, 2018]:

$$G(\phi_i) = \mathbb{E}_{\mathbf{s}_{\mathcal{N}_i}, \mathbf{a}_{\mathcal{N}_i} \sim \mathcal{D}_i} \left[\nabla_{\phi_i} \mu_i(\mathbf{s}_{\mathcal{N}_i}) \nabla_{a_i} \tilde{Q}_i^{\mu}(\mathbf{s}_{\mathcal{N}_i}, \mathbf{a}_{\mathcal{N}_i}) \right], \quad (2)$$

where again data \mathcal{D}_i only from local interactions is needed.

5.2 Distributed Learning with Local Interactions

To implement the parameter updates proposed above, agent i needs training data $\mathcal{D}_i = (\mathbf{s}_{\mathcal{N}_i}, \mathbf{a}_{\mathcal{N}_i}, r_i, \{\mathbf{s}_{\mathcal{N}'_j}\}_{j \in \mathcal{N}'_i})$ from its one-hop neighbors at the current and next time steps, whose dynamics obey the following proposition (see proof in Appendix A.2).

Proposition 1. *Under Assumption 1, if an agent j is not a potential neighbor of agent i at time t , i.e., $j \notin \mathcal{P}_i(t)$, it will not be a one-hop neighbor of agent i at time $t + 1$, i.e., $j \notin \mathcal{N}_i(t + 1)$.*

Proposition 1 allows us to decouple the global interactions among agents and limit message exchanges or observations to be among one-hop neighbors. It also allows parallel training on a distributed computing architecture, where each compute node only needs to simulate a small subset of the agents. This leads to significant training efficiency gains as demonstrated in Sec. 6.

To collect training data, at each time step, agent i first interacts with its one-hop neighbors to obtain their states $\mathbf{s}_{\mathcal{N}_i}$ and actions $\mathbf{a}_{\mathcal{N}_i}$ and compute its reward $r_i(\mathbf{s}_{\mathcal{N}_i}, \mathbf{a}_{\mathcal{N}_i})$. To obtain $\mathbf{s}_{\mathcal{N}'_j}$ for all $j \in \mathcal{N}'_i$, we first determine agent i 's one-hop neighbors at the next time step, \mathcal{N}'_i . Using Proposition 1, we let each potential neighbor $k \in \mathcal{P}_i$ perform a transition to a new state $s'_k \sim p_k(\cdot | \mathbf{s}_{\mathcal{N}_k}, a_k)$, which is sufficient to determine \mathcal{N}'_i . Then, we let the potential neighbors \mathcal{P}_j of each new neighbor $j \in \mathcal{N}'_i$ perform transitions to determine \mathcal{N}'_j and obtain $\mathbf{s}_{\mathcal{N}'_j}$. Fig. 1(a) illustrates the data collection process. At time t , agent i obtains $\mathbf{s}_{\mathcal{N}_i}$, $\mathbf{a}_{\mathcal{N}_i}$, and $r_i(\mathbf{s}_{\mathcal{N}_i}, \mathbf{a}_{\mathcal{N}_i})$ for $\mathcal{N}_i = \{i, 1\}$. Then, the potential neighbors of agent i , $\mathcal{P}_i = \{1, 2, i\}$, proceed to their next states at time $t + 1$. This is sufficient to determine that $\mathcal{N}'_i = \{i, 2\}$ and obtain $\mathbf{s}_{\mathcal{N}'_i}$. Finally, we let agent 3, which belongs to set $\mathcal{P}_2 = \{i, 1, 2, 3\}$, perform a transition to determine that $\mathcal{N}'_2 = \{i, 2, 3\}$ and obtain $\mathbf{s}_{\mathcal{N}'_2}$.

We now describe a distributed learning framework that exploits the local interactions among the agents to optimize the policy and Q function parameters. Our training framework consists of a central controller and M learners, each training a different agent. The central controller stores a copy of all policy and target policy parameters, $\phi_m, \hat{\phi}_m, \forall m \in [M]$. In each training iteration, the central controller broadcasts the parameters to all learners. Each learner i updates its own policy parameters $\phi_i, \hat{\phi}_i$ and returns the updated values to the central controller.

Each learner i maintains the parameters θ_i and $\hat{\theta}_i$ of agent i 's approximated Q and target Q function. In each training iteration, learner i uses policies with parameters $\{\phi_m, \hat{\phi}_m\}_{m \in [M]}$

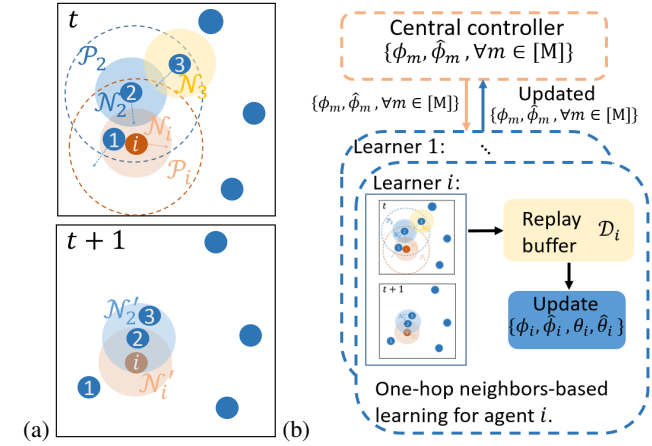


Fig. 1: (a) One-hop neighbor transitions from one time step to the next in a d -disk proximity graph; (b) Distributed MARL with local interactions.

received from the central controller. Transitions are simulated only for agent i , its potential neighbors \mathcal{P}_i , and the potential neighbors \mathcal{P}_j of each new neighbor $j \in \mathcal{N}'_i$ as described above. DARN1N achieves significant computation savings because (i) the Q function parameters θ_i and $\hat{\theta}_i$ are stored locally at each learner i and do not need to be communicated, and (ii) the agent transition simulation occurs only over small groups of agents, distributed among the M learners instead of centralized over all agents at the central controller. The interaction data $(\mathbf{s}_{\mathcal{N}_i}, \mathbf{a}_{\mathcal{N}_i}, r_i, \{\mathbf{s}_{\mathcal{N}'_j}\}_{j \in \mathcal{N}'_i})$ are stored in the replay buffer \mathcal{D}_i . Finally, learner i updates θ_i and ϕ_i using (1) and (2), respectively, and the target network parameters $\hat{\theta}_i$ and $\hat{\phi}_i$ via Polyak averaging. Fig. 1(b) illustrates the distributed training procedure. The pseudocode of DARN1N is provided in Alg. 1.

6 Experiments

In this section, we conduct experiments to evaluate the performance of DARN1N.

6.1 Experiment Settings

Environments We evaluate DARN1N in four environments, Ising Model [Yang *et al.*, 2018], Food Collection, Grassland, and Adversarial Battle [Long *et al.*, 2020], which cover cooperative and mixed cooperative competitive games. The details of each environment are described in Appendix A.3.

Benchmarks and Evaluation Metrics We compare our method with three state-of-the-art MARL algorithms: MADDPG [Lowe *et al.*, 2017], MFAC [Yang *et al.*, 2018], and EPC [Long *et al.*, 2020], and evaluate them using two criteria: *training efficiency* and *policy quality*. To measure the training efficiency, we use two metrics: 1) *average training time* spent to run a specified number of training iterations and 2) *convergence time*. The convergence time is defined as the time when the variance of the average total training reward over 90 consecutive iterations does not exceed 2% of the absolute mean reward, where the average total training reward is the total reward of all agents averaged over 10 episodes in three training runs with different random seeds. To measure policy

Algorithm 1: DARL1N: Distributed multi-Agent Reinforcement Learning with One-hop Neighbors

```

// Central controller:
1 Initialize policy, target policy parameters  $\phi = \{\phi_m, \hat{\phi}_m\}_{m \in [M]}$ .
2 Broadcast  $\phi$  to the learners.
3 do
4   Listen to channel and collect updated  $\phi$  from learners.
5 while updated  $\phi$  is not received;
// Learner  $i$ :
6 Initialize parameters  $\theta_i, \hat{\theta}_i$  of  $\tilde{Q}_i^\mu, \hat{Q}_i^\mu$  and replay buffer  $\mathcal{D}_i$ .
7 for  $iter = 1 : max\_iteration$  do
8   Listen to channel.
9   if  $\phi$  received from the central controller then
10    // Local interactions:
11    for  $step = 1 : max\_transition\_number$  do
12      Randomly initialize all agent states.
13      Simulate one-step transitions for the potential
14      neighbors  $\mathcal{P}_i$  of agent  $i$  to determine  $\mathcal{N}'_i$ .
15      Simulate one-step transitions for the potential
16      neighbors  $\mathcal{P}_j$  of each agent  $j \in \mathcal{N}'_i$  to get  $\mathbf{s}_{\mathcal{N}'_i}$ .
17      Store the obtained local interactions
18       $(\mathbf{s}_{\mathcal{N}_i}, \mathbf{a}_{\mathcal{N}_i}, r_i, \{\mathbf{s}_{\mathcal{N}'_j}\}_{j \in \mathcal{N}'_i})$  in the buffer  $\mathcal{D}_i$ .
19    // One-hop neighbor-based learning:
20    Sample a mini-batch from  $\mathcal{D}_i$  and update  $\phi_i, \theta_i, \hat{\phi}_i, \hat{\theta}_i$ .
21    Send updated  $\phi_i, \hat{\phi}_i$  to the central controller.

```

quality, we use *convergence reward*, which is the average total training reward at the convergence time.

Experiment Configurations We run our experiments on Amazon EC2 computing clusters [AWS, 2022]. To understand the scalability of each method, for each environment, we consider four scenarios with increasing number of agents. The number of agents in the Ising Model and Food Collection environments are set to $M = 9, 16, 25, 64$ and $M = 3, 6, 12, 24$, respectively. In the Grassland and Adversarial Battle environments, the number of agents are set to $M = 6, 12, 24, 48$.

To evaluate the training efficiency, we configure the computing resources used to train each method in a way so that DARL1N utilizes roughly the same or fewer resources. In particular, to train DARL1N, Amazon EC2 instance *c5n.large* is used in all scenarios for all environments. To train MADDPG and MFAC, instance *z1d.3xlarge* is used in the first scenario ($M = 9$) for Ising Model and in the first two scenarios for Food Collection, Grassland and Adversarial Battle. In the other scenarios, instance *z1d.6xlarge* is used. To train EPC, we use instance *c5.12xlarge* in all scenarios for Food Collection and in the first three scenarios for Ising Model, Grassland and Adversarial Battle. The other scenarios adopt instance *c5.18xlarge*. To configure the parallel computing architecture in EPC, we set the number of parallel computing instances and the number of independent environments to 3 and 25, respectively. More configuration details including the configurations of the selected Amazon EC2 instances are provided in Appendix A.4.

Method	Convergence Time (s)				Convergence Reward			
	$M = 9$	16	25	64	9	16	25	64
MADDPG	62	263	810	1996	460	819	1280	1831
MFAC	63	274	851	2003	468	814	1276	1751
EPC	101	26	51	62	468	831	1278	3321
EPC Scratch	101	412	993	2995	468	826	1275	2503
DARL1N	38	102	210	110	465	828	1279	2282

Tab. 1: Convergence time and convergence reward of different methods in the Ising Model environment.

Method	Convergence Time (s)				Convergence Reward			
	$M = 3$	6	12	24	3	6	12	24
MADDPG	501	1102	4883	2005	24	24	-112	-364
MFAC	512	832	4924	2013	20	23	-115	-362
EPC	1314	723	2900	8104	19	11	8	-2
DARL1N	502	480	310	730	14	25	43	61

Tab. 2: Convergence time and convergence reward of different methods in the Food Collection environment.

6.2 Experiment Results

This section presents the main experiment results. Other results, including 1) training reward of each method in different environments, 2) visualizations of the trained agents playing different games, and 3) the money spent for training each method are included in Appendix A.5 due to space limitations.

Ising Model Tab. 1 shows the convergence reward and convergence time of different methods. When the number of agents is small ($M = 9$), all methods achieve roughly the same reward. DARL1N takes the least amount of time to converge while EPC takes the longest time. When the number of agents increases, it can be observed that the EPC converges immediately and the convergence reward it achieves when $M = 64$ is much higher than the other methods. The reason is that, in the Ising Model, each agent only needs information of its four fixed neighbors, and hence in EPC the policy obtained from the previous stage can be applied to the current stage. The other methods train the agents from scratch without curriculum learning. For illustration, we also show the convergence reward and convergence time achieved by training EPC from scratch without curriculum learning (denoted as EPC Scratch in Tab. 1). The results show that EPC Scratch converges much slower than EPC as the number of agents increases. Note that when the number of agents is 9, EPC and EPC Scratch are the same. Moreover, DARL1N achieves a reward comparable with that of EPC Scratch but converges much faster.

Fig. 2(a) shows the average time taken to train each method for 10 iterations in different scenarios. DARL1N requires much less time to perform a training iteration than the benchmark methods.

Food Collection The convergence rewards and convergence times in this environment are shown in Tab. 2. The results show that, when the problem scale is small, DARL1N, MADDPG and MFAC achieve similar performance in terms of policy quality. As the problem scale increases, the performance of MADDPG and MFAC degrades significantly and becomes much worse than DARL1N or EPC when $M = 12$ and $M = 24$, which is also shown in Figs. 3(a)-3(b). The convergence

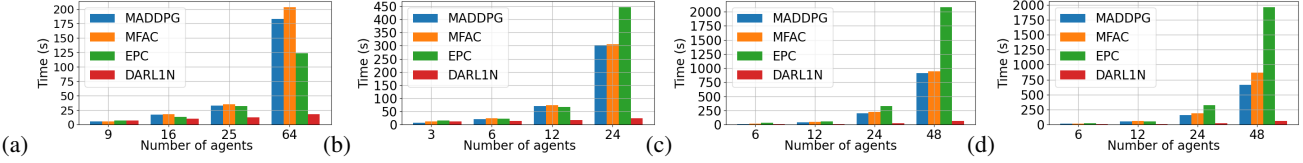


Fig. 2: Average training time of different methods to run (a) 10 iterations in the Ising Model, (b) 30 iterations in the Food Collection, (c) 30 iterations in the Grassland, and (d) 30 iterations in the Adversarial Battle environments.

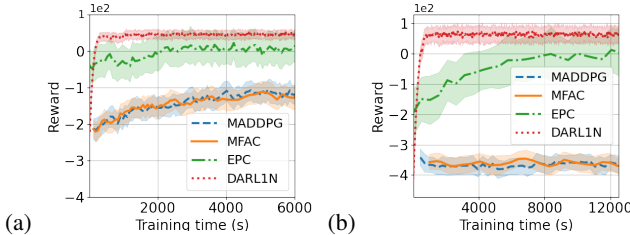


Fig. 3: Average total training reward of different methods in the Food Collection environment when there are (a) $M = 12$, (b) $M = 24$ agents.

Method	Convergence Time (s)				Convergence Reward			
	$M = 6$	12	24	48	6	12	24	48
MADDPG	423	6271	2827	1121	21	11	-302	-612
MFAC	431	7124	3156	1025	23	9	-311	-608
EPC	4883	2006	3324	15221	12	38	105	205
DARL1N	103	402	1752	5221	18	46	113	210

Tab. 3: Convergence time and convergence reward of different methods in the Grassland environment.

reward achieved by DARL1N is comparable or sometimes higher than that achieved by EPC. Moreover, the convergence speed of DARL1N is the highest among all methods in all scenarios.

Fig. 2(b) shows the average training time for running 30 iterations. Similar as the results obtained in the Ising Model, DARL1N achieves the highest training efficiency and its training time grows linearly as the number of agents increases. When $M = 24$, EPC takes the longest training time. This is because of the complex policy and Q neural network architectures in EPC, the input dimensions of which grow linearly and quadratically, respectively, with more agents.

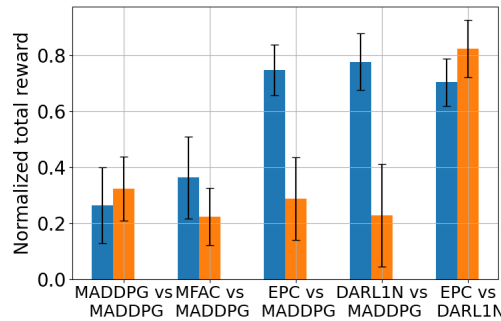


Fig. 4: Mean and standard deviation of normalized total reward of competing agents trained by different methods in the Adversarial Battle environment with $M = 48$.

Method	Convergence Time (s)				Convergence Reward			
	$M = 6$	12	24	48	6	12	24	48
MADDPG	452	1331	1521	7600	-72	-211	-725	-1321
MFAC	463	1721	1624	6234	-73	-221	-694	-1201
EPC	1512	1432	2041	9210	-75	-215	-405	-642
DARL1N	121	756	1123	3110	-71	-212	-410	-682

Tab. 4: Convergence time and convergence reward of different methods in the Adversarial Battle environment.

Grassland Similar as the results in the Food Collection environment, the policy generated by DARL1N is equally good or even better than those generated by the benchmark methods, as shown in Tab. 3 and Fig. 2(c), especially when the problem scale is large. DARL1N also has the fastest convergence speed and takes the shortest time to run a training iteration.

Adversarial Battle In this environment, DARL1N again achieves good performance in terms of policy quality and training efficiency compared to the baseline methods, as shown in Tab. 4 and Fig. 2(d). To further evaluate the performance, we reconsider the last scenario ($M = 48$) and train the good agents and adversary agents using two different methods. The trained good agents and adversarial agents are then compete with each other in the environment. We then apply the Min-Max normalization to measure the normalized total reward of agents at each side achieved in an episode. To reduce uncertainty, we generate 10 episodes and record the mean values and standard deviations. As shown in Fig. 4, DARL1N achieves the best performance, and both DARL1N and EPC significantly outperform MADDPG and MFAC.

7 Conclusion

This paper introduces DARL1N, a scalable MARL algorithm. DARL1N features a novel training scheme that breaks the curse of dimensionality for action value function approximation by restricting the interactions among agents within one-hop neighborhoods. This reduces the learning complexity and enables fully distributed and parallel training, in which individual compute nodes only simulate interactions among a small subset of agents. To demonstrate the scalability and training efficiency of DARL1N, we conducted comprehensive evaluation in comparison with three state-of-the-art MARL algorithms, MADDPG, MFAC, and EPC. The results show that DARL1N generates equally good or even better policies in almost all scenarios with significantly higher training efficiency than benchmark methods, especially in large-scale problem settings.

References

[AWS, 2022] AWS. Amazon ec2. <https://aws.amazon.com/ec2/>, 2022. Accessed: 2022-01-13.

[Babaeizadeh *et al.*, 2017] Mohammad Babaeizadeh, Iuri Frosio, Stephen Tyree, Jason Clemons, and Jan Kautz. Reinforcement learning through asynchronous advantage actor-critic on a gpu. In *International Conference on Learning Representations (ICLR)*, 2017.

[Böhmer *et al.*, 2020] Wendelin Böhmer, Vitaly Kurin, and Shimon Whiteson. Deep coordination graphs. In *International Conference on Machine Learning*, pages 980–991. PMLR, 2020.

[Bullo *et al.*, 2009] Francesco Bullo, Jorge Cortés, and Sonia Martinez. *Distributed control of robotic networks: a mathematical approach to motion coordination algorithms*. Princeton University Press, 2009.

[Buşoniu *et al.*, 2010] Lucian Buşoniu, Robert Babuška, and Bart De Schutter. Multi-agent reinforcement learning: An overview. *Innovations in Multi-agent Systems and Applications*, pages 183–221, 2010.

[Chen *et al.*, 2018] Tianyi Chen, Kaiqing Zhang, Georgios B Giannakis, and Tamer Başar. Communication-efficient distributed reinforcement learning. *arXiv preprint arXiv:1812.03239*, 2018.

[Chu *et al.*, 2019] Tianshu Chu, Jie Wang, Lara Codecà, and Zhaojian Li. Multi-agent deep reinforcement learning for large-scale traffic signal control. *IEEE Transactions on Intelligent Transportation Systems*, 21(3):1086–1095, 2019.

[Foerster *et al.*, 2018] Jakob Foerster, Gregory Farquhar, Triantafyllos Afouras, Nantas Nardelli, and Shimon Whiteson. Counterfactual multi-agent policy gradients. In *AAAI Conference on Artificial Intelligence*, volume 32, 2018.

[Iqbal and Sha, 2019] Shariq Iqbal and Fei Sha. Actor-attention-critic for multi-agent reinforcement learning. In *International Conference on Machine Learning*, pages 2961–2970. PMLR, 2019.

[Kuyer *et al.*, 2008] Lior Kuyer, Shimon Whiteson, Bram Bakker, and Nikos Vlassis. Multiagent reinforcement learning for urban traffic control using coordination graphs. In *Joint European Conference on Machine Learning and Knowledge Discovery in Databases*, pages 656–671. Springer, 2008.

[Lillicrap *et al.*, 2016] Timothy P. Lillicrap, Jonathan J. Hunt, Alexander Pritzel, Nicolas Heess, Tom Erez, Yuval Tassa, David Silver, and Daan Wierstra. Continuous control with deep reinforcement learning. In *International Conference on Learning Representations (ICLR)*, 2016.

[Lin *et al.*, 2020] Yiheng Lin, Guannan Qu, Longbo Huang, and Adam Wierman. Distributed reinforcement learning in multi-agent networked systems. *arXiv preprint arXiv:2006.06555*, 2020.

[Long *et al.*, 2020] Qian Long, Zihan Zhou, Abhibav Gupta, Fei Fang, Yi Wu, and Xiaolong Wang. Evolutionary population curriculum for scaling multi-agent reinforcement learning. In *International Conference on Learning Representations (ICLR)*, 2020.

[Lowe *et al.*, 2017] Ryan Lowe, Yi I Wu, Aviv Tamar, Jean Harb, OpenAI Pieter Abbeel, and Igor Mordatch. Multi-agent actor-critic for mixed cooperative-competitive environments. In *Advances in neural information processing systems*, pages 6379–6390, 2017.

[Mnih *et al.*, 2016] Volodymyr Mnih, Adria Puigdomenech Badia, Mehdi Mirza, Alex Graves, Timothy Lillicrap, Tim Harley, David Silver, and Koray Kavukcuoglu. Asynchronous methods for deep reinforcement learning. In *International conference on machine learning*, pages 1928–1937, 2016.

[Nair *et al.*, 2015] Arun Nair, Praveen Srinivasan, Sam Blackwell, Cagdas Alcicek, Rory Fearon, Alessandro De Maria, Vedavyas Panneershelvam, Mustafa Suleyman, Charles Beattie, Stig Petersen, et al. Massively parallel methods for deep reinforcement learning. In *International Conference on Machine Learning (ICML)*, 2015.

[OpenAI, 2022] OpenAI. A2C. <https://openai.com/blog/baselines-acktr-a2c/>, 2022. Accessed: 2022-01-13.

[Qu *et al.*, 2020] Guannan Qu, Adam Wierman, and Na Li. Scalable reinforcement learning of localized policies for multi-agent networked systems. In *Learning for Dynamics and Control*, pages 256–266. PMLR, 2020.

[Rashid *et al.*, 2018] Tabish Rashid, Mikayel Samvelyan, Christian Schroeder, Gregory Farquhar, Jakob Foerster, and Shimon Whiteson. Qmix: Monotonic value function factorisation for deep multi-agent reinforcement learning. In *International Conference on Machine Learning*, pages 4295–4304. PMLR, 2018.

[Simões *et al.*, 2020] David Simões, Nuno Lau, and Luís Paulo Reis. Multi-agent actor centralized-critic with communication. *Neurocomputing*, 2020.

[Son *et al.*, 2019] Kyunghwan Son, Daewoo Kim, Wan Ju Kang, David Earl Hostallero, and Yung Yi. Qtran: Learning to factorize with transformation for cooperative multi-agent reinforcement learning. In *International Conference on Machine Learning*, pages 5887–5896. PMLR, 2019.

[Sunehag *et al.*, 2017] Peter Sunehag, Guy Lever, Audrunas Gruslys, Wojciech Marian Czarnecki, Vinicius Zambaldi, Max Jaderberg, Marc Lanctot, Nicolas Sonnerat, Joel Z Leibo, Karl Tuyls, et al. Value-decomposition networks for cooperative multi-agent learning. *arXiv preprint arXiv:1706.05296*, 2017.

[Sutton and Barto, 2018] Richard S Sutton and Andrew G Barto. *Reinforcement Learning: An Introduction*. MIT Press, 2018.

[Yang *et al.*, 2018] Yaodong Yang, Rui Luo, Minne Li, Ming Zhou, Weinan Zhang, and Jun Wang. Mean field multi-agent reinforcement learning. In *International Conference on Machine Learning*, pages 5571–5580. PMLR, 2018.

A Appendix

A.1 Proof of Lemma 1

Proof. The proof of Lemma 1 is similar to the proofs for Lemmas 3-4 in [Qu *et al.*, 2020] on SAC. The difference is that DARN1 uses a more general reward function $r_i(\mathbf{s}_{\mathcal{N}_i}, \mathbf{a}_{\mathcal{N}_i})$ compared with the function $r_i(s_i, a_i)$ used in SAC. Moreover, the constraint $r_i > 0$ in SAC is removed in our method.

To prove Lemma 1, we first prove the following inequality

$$|Q_i^\mu(s_{\mathcal{N}_i}, s_{\mathcal{N}_i^-}, a_{\mathcal{N}_i}, a_{\mathcal{N}_i^-}) - Q_i^\mu(s_{\mathcal{N}_i}, \hat{s}_{\mathcal{N}_i^-}, a_{\mathcal{N}_i}, \hat{a}_{\mathcal{N}_i^-})| \leq \frac{2\bar{r}\gamma}{1-\gamma} \quad (3)$$

where $\hat{s}_{\mathcal{N}_i^-} \neq s_{\mathcal{N}_i^-}$ and $\hat{a}_{\mathcal{N}_i^-} \neq a_{\mathcal{N}_i^-}$. Particularly, letting (\mathbf{s}, \mathbf{a}) and $(\hat{\mathbf{s}}, \hat{\mathbf{a}})$ denote $(s_{\mathcal{N}_i}, s_{\mathcal{N}_i^-}, a_{\mathcal{N}_i}, a_{\mathcal{N}_i^-})$ and $(s_{\mathcal{N}_i}, \hat{s}_{\mathcal{N}_i^-}, a_{\mathcal{N}_i}, \hat{a}_{\mathcal{N}_i^-})$, respectively, we have

$$\begin{aligned} & |Q_i^\mu(\mathbf{s}, \mathbf{a}) - Q_i^\mu(\hat{\mathbf{s}}, \hat{\mathbf{a}})| \\ &= |\mathbb{E}[\sum_{t=0}^{\infty} \gamma^t r_i(s_{\mathcal{N}_i}(t), a_{\mathcal{N}_i}(t)) \mid (\mathbf{s}(0), \mathbf{a}(0)) = (\mathbf{s}, \mathbf{a})] \\ &\quad - \mathbb{E}[\sum_{t=0}^{\infty} \gamma^t r_i(s_{\mathcal{N}_i}(t), a_{\mathcal{N}_i}(t)) \mid (\mathbf{s}(0), \mathbf{a}(0)) = (\hat{\mathbf{s}}, \hat{\mathbf{a}})]| \\ &\leq \sum_{t=0}^{\infty} |\mathbb{E}[\gamma^t r_i(s_{\mathcal{N}_i}(t), a_{\mathcal{N}_i}(t)) \mid (\mathbf{s}(0), \mathbf{a}(0)) = (\mathbf{s}, \mathbf{a})] \\ &\quad - \mathbb{E}[\gamma^t r_i(s_{\mathcal{N}_i}(t), a_{\mathcal{N}_i}(t)) \mid (\mathbf{s}(0), \mathbf{a}(0)) = (\hat{\mathbf{s}}, \hat{\mathbf{a}})]| \\ &\stackrel{(a)}{=} \sum_{t=1}^{\infty} |\mathbb{E}[\gamma^t r_i(s_{\mathcal{N}_i}(t), a_{\mathcal{N}_i}(t)) \mid (\mathbf{s}(0), \mathbf{a}(0)) = (\mathbf{s}, \mathbf{a})] \\ &\quad - \mathbb{E}[\gamma^t r_i(s_{\mathcal{N}_i}(t), a_{\mathcal{N}_i}(t)) \mid (\mathbf{s}(0), \mathbf{a}(0)) = (\hat{\mathbf{s}}, \hat{\mathbf{a}})]| \\ &\leq \sum_{t=1}^{\infty} \gamma^t (|\mathbb{E}[r_i(s_{\mathcal{N}_i}(t), a_{\mathcal{N}_i}(t)) \mid (\mathbf{s}(0), \mathbf{a}(0)) = (\mathbf{s}, \mathbf{a})]| \\ &\quad + |\mathbb{E}[r_i(s_{\mathcal{N}_i}(t), a_{\mathcal{N}_i}(t)) \mid (\mathbf{s}(0), \mathbf{a}(0)) = (\hat{\mathbf{s}}, \hat{\mathbf{a}})]|) \\ &\leq \sum_{t=1}^{\infty} 2\gamma^t \bar{r} \\ &= \frac{2\bar{r}\gamma}{1-\gamma} \end{aligned} \quad (4)$$

where (a) derives from the fact that $(s_{\mathcal{N}_i}, a_{\mathcal{N}_i})$ are part of both (\mathbf{s}, \mathbf{a}) and $(\hat{\mathbf{s}}, \hat{\mathbf{a}})$. In the above equations, we have removed the subscription of the expectation function $\mathbb{E}()$ for simplicity, which should be $\mathbf{a}(t) = \mu(\mathbf{s}(t)), \mathbf{s}(t) \sim p$.

Then we have

$$\begin{aligned} & |\tilde{Q}_i^\mu(\mathbf{s}_{\mathcal{N}_i}, \mathbf{a}_{\mathcal{N}_i}) - Q_i^\mu(\mathbf{s}, \mathbf{a})| \\ &= \left| \sum_{\mathbf{s}_{\mathcal{N}_i^-}, \mathbf{a}_{\mathcal{N}_i^-}} \omega_i(\mathbf{s}_{\mathcal{N}_i}, \mathbf{a}_{\mathcal{N}_i}, \mathbf{s}_{\mathcal{N}_i^-}, \mathbf{a}_{\mathcal{N}_i^-}) Q_i^\mu(\mathbf{s}_{\mathcal{N}_i}, \mathbf{a}_{\mathcal{N}_i}, \mathbf{s}_{\mathcal{N}_i^-}, \mathbf{a}_{\mathcal{N}_i^-}) \right. \\ &\quad \left. - Q_i^\mu(\mathbf{s}_{\mathcal{N}_i}, \mathbf{a}_{\mathcal{N}_i}, \hat{\mathbf{s}}_{\mathcal{N}_i^-}, \hat{\mathbf{a}}_{\mathcal{N}_i^-}) \right| \\ &\leq \sum_{\mathbf{s}_{\mathcal{N}_i^-}, \mathbf{a}_{\mathcal{N}_i^-}} \omega_i(\mathbf{s}_{\mathcal{N}_i}, \mathbf{a}_{\mathcal{N}_i}, \mathbf{s}_{\mathcal{N}_i^-}, \mathbf{a}_{\mathcal{N}_i^-}) |Q_i^\mu(\mathbf{s}_{\mathcal{N}_i}, \mathbf{a}_{\mathcal{N}_i}, \mathbf{s}_{\mathcal{N}_i^-}, \mathbf{a}_{\mathcal{N}_i^-}) \\ &\quad - Q_i^\mu(\mathbf{s}_{\mathcal{N}_i}, \mathbf{a}_{\mathcal{N}_i}, \hat{\mathbf{s}}_{\mathcal{N}_i^-}, \hat{\mathbf{a}}_{\mathcal{N}_i^-})| \\ &\leq \frac{2\bar{r}\gamma}{1-\gamma} \end{aligned}$$

The proof is complete now. \square

A.2 Proof of Proposition 1

Proof. If agent $j \notin \mathcal{P}_i(t)$, then based on the definition of potential neighbors, we have $dist(\mathbf{s}_i(t), \mathbf{s}_j(t)) > d + 2\epsilon$. According to the triangle inequality, $dist(\mathbf{s}_i(t), \mathbf{s}_j(t+1)) + dist(\mathbf{s}_j(t+1), \mathbf{s}_j(t)) \geq dist(\mathbf{s}_i(t), \mathbf{s}_j(t))$, and according to Assumption 1, $dist(\mathbf{s}_j(t+1), \mathbf{s}_j(t)) \leq \epsilon$. Therefore, $dist(\mathbf{s}_i(t), \mathbf{s}_j(t+1)) > d + \epsilon$. Furthermore, using triangle inequality, we can obtain $dist(\mathbf{s}_i(t+1), \mathbf{s}_j(t+1)) + dist(\mathbf{s}_i(t+1), \mathbf{s}_i(t)) \geq dist(\mathbf{s}_i(t), \mathbf{s}_j(t+1))$. As $dist(\mathbf{s}_i(t+1), \mathbf{s}_i(t)) \leq \epsilon$, we have $dist(\mathbf{s}_i(t+1), \mathbf{s}_j(t+1)) > d$. Therefore, agent j will not be a one-hop neighbor of agent i at time $t+1$. \square

A.3 Environment Details

Ising Model The Ising Model captures the ferromagnetism property in statistical mechanics. The environment contains M spins (agents) arranged in a lattice with state 1 or -1 . A spin tends to align with its neighbors to minimize energy by choosing to spin up (+1) or down (-1). The reward of each agent is given by $r_i = \frac{\lambda}{2} \sum_{k \in \mathcal{N}_i} a_i a_k$, where λ is an environment parameter and is set to $\lambda = 1$. The one-hop neighbors of agent i , \mathcal{N}_i , are defined as the agents that are horizontally or vertically adjacent to agent i including agent i itself. In addition, agents at the boundary on one side can be the neighbors of agents at the boundary on the other side. Therefore, each agent has exactly 5 neighbors including itself.

Food Collection In this environment, M agents are tasked to reach as many out of M food locations as possible while avoiding collisions with each other. An agent gets a positive reward when it reaches a food location and a negative reward when it collides with another agent. Each agent gets +1 reward when it reaches a food location and gets -1 reward when it collides with another agent. Moreover, to drive agents to reach food locations, each agent gets less negative reward when it is closer to a food location.

Grassland This environment consists of K good agents (sheep) and $M - K$ adversary agents (wolf). The good agents aim to collect L grass pellets. Once a grass pellet is collected, the good agent gets a positive reward and a new grass pellet is generated randomly. The adversary agents chase the good agents and get positive rewards when colliding with (eating) the good agents, at which time the good agents get negative

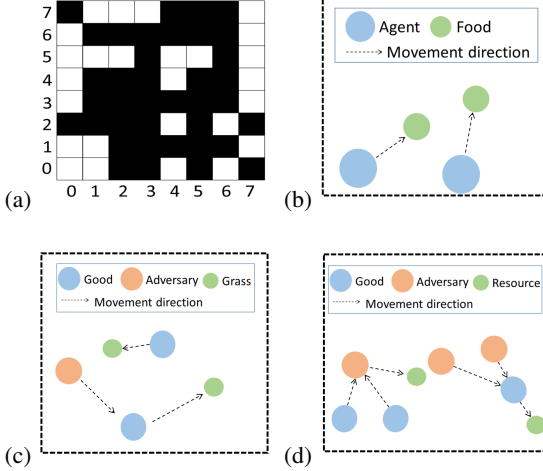


Fig. 5: Illustration of the four environments: a) Ising Model, b) Food Collection, c) Grassland, d) Adversarial Battle.

rewards. In this environment, we only evaluate the training of good agents, as adversary agents need to know the global states of agents and hence cannot be trained using DARN1N. Each good agent gets +20 reward when it collects a grass pellet and gets -5 reward when colliding with an adversary agent. Each adversary agent gets +15 reward when it collides with a good agent. Similar to Food Collection, each good agent gets less negative reward when it is closer to a grass pellet, and each adversary agent gets less negative reward when it is closer to a good agent.

Adversarial Battle In Adversarial Battle, there are $\frac{M}{2}$ good agents and $\frac{M}{2}$ adversary agents competing for P units of resources. Each agent gets a positive reward when a resource is collected. When more than two good agents collide with an adversary agent, the good agents get positive rewards and the adversary agent gets a negative reward and becomes deactivated, and vice versa. Since the adversary agents and good agents are exchangeable, we only evaluate the training of good agents. Each agent gets +10 reward when it collects a resource unit and gets -5 reward when it is killed. Moreover, when an agent kills an agent from the other team by collaborating with other agents in the same team, this agent gets +5 reward. To encourage agents to collect resource units and battle with agents from the other team, each agent gets less negative reward when it is closer to a resource unit or closer to any agent from the other team.

In our experiments, the number of adversary agents K , grass pellets L and resource units P are all set to $\frac{M}{2}$, and all adversary agents adopt policies trained by MADDPG.

A.4 Experiment Settings

Training Parameters All environments adopt the same training parameters. In particular, Adam optimizer is used to update the policy and Q function parameters with a learning rate of 0.01. The parameter τ in the Polyak averaging algorithm for updating target policy and target Q functions is set to $\tau = 0.01$. The discount factor γ is set to $\gamma = 0.95$. The size

Instances	CPU cores	CPU frequency	Memory	Network	Hourly price
<i>c5n.large</i>	2	3.4 GHz	5.3 GB	≤ 25 Gb	\$ 0.108
<i>z1d.3xlarge</i>	12	4 GHz	96 GB	≤ 10 Gb	\$ 1.116
<i>z1d.6xlarge</i>	24	4 GHz	192 GB	≤ 10 Gb	\$ 2.232
<i>c5.12xlarge</i>	48	3.6 GHz	96 GB	12 Gb	\$ 2.04
<i>c5.18xlarge</i>	72	3.6 GHz	144 GB	25 Gb	\$ 3.06

Tab. 5: Configurations of Amazon EC2 instances

of the buffer is set to 10^6 . The parameters are updated after every 4 episodes. The $\max_transition_number$ in Alg. 1 of DARN1N is set to 4 times of the length of one episode. In the Ising Model and Food Collection environments, the length of each episode is set to 25 in all scenarios. In the Grassland and Adversarial Battle environments, the length of an episode is set to 25, 30, 35 and 40 for the scenarios of $M = 6, 12, 24$ and 48, respectively. The size of a mini batch is set to 32 in the Ising Model and 1024 in other environments.

Q Function and Policy Function Representation In the implementations of DARN1N, MADDPG and MFAC, we use neural networks with fully connected layers to represent the approximated Q function and policy function. The neural networks have three hidden layers with each layer having 64 units and adopting ReLU as the activation function. To handle the varying sizes of $\mathbf{s}_{\mathcal{N}_i}$ and $\mathbf{a}_{\mathcal{N}_i}$ in approximated Q function in DARN1N, we let the input dimension of the approximated Q function to be the size of the joint state and action space of the maximum number of agents that can be in \mathcal{N}_i and apply zero padding for agents that are not in the one-hop neighborhood of agent i . In particular, in the Ising Model, the maximum number of one-hop neighbors of an agent is 4, which is fixed. The input dimension of the approximated Q function for agent i is then $4 \times (|\mathcal{S}_i| + |\mathcal{A}_i|)$. For other environments, the maximum number of one-hop neighbors of an agent is the total number of agents. The EPC adopts a population-invariant neural network architecture with attention modules to support arbitrary number of agents in different stages for training the Q function and policy function [Long *et al.*, 2020].

Environment and Neighborhood Configurations The one-hop neighbors of an agent are defined over the agent's state space using a distance metric. In the Ising Model, the topology of the agents is fixed, and the one-hop neighbors of an agent are its vertically and horizontally adjacent agents. In the other environments, the Euclidean distance between two agents in the 2-D space is used as the distance metric, and the neighbor distance d is set to 0.15, 0.2, 0.25, 0.3, 0.35 when $M = 3, 6, 12, 24, 48$, respectively. The bound ϵ is determined according to the maximum velocity and time interval between two consecutive time steps, and is set to 0.05, 0.10, 0.15, 0.20, 0.25 when $M = 3, 6, 12, 24, 48$, respectively. The size of agents' activity space is set to $[-1, 1] \times [-1, 1], [-1.5, 1.5] \times [-1.5, 1.5], [-2, 2] \times [-2, 2], [-2.5, 2.5] \times [-2.5, 2.5], [-3, 3] \times [-3, 3]$ when $M = 3, 6, 12, 24, 48$, respectively.

Compute Nodes The configurations of Amazon EC2 instances as the compute nodes are summarized in Tab. 5.

A.5 Additional Experiment Results

Training Curves The average total training reward versus the training time of different methods in different environments are shown in Figs. 6-9. As we can see, when the number of agents is small as shown in Figs. 6(a), 7(a), 8(a), 8(a), all methods converge to roughly the same reward level. DARL1N has the fastest convergence speed, and EPC is the slowest. Moreover, in the Ising Model, with the increase of the number of agents, EPC achieves the best performance and converges immediately without further training due to curriculum learning as shown in Figs. 6(b), 6(c), 6(d). However, our method converges much faster than EPC trained from scratch without curriculum learning as shown in Fig. 6. In the other environments, when the number of agents increases, both EPC and our method achieve a high reward, but the performance of MADDPG and MFAC degrades significantly, as shown in Figs. 7(c), 7(d), 8(c), 8(d), 9(c), 9(d). Moreover, DARL1N again achieves the highest training efficiency.

Training Costs To evaluate the training cost of each method, we measure the money spent for training each method based on the configurations described in the Experiments section. Tab. 6-8 show the hourly price rate for training each method, and Fig. 10 shows the total money spent for training in different scenarios and different environments.

Tab. 6: Hourly price rate for training each method in the Ising Model.

Method	Hourly Price Rate			
	$M = 9$	$M = 16$	$M = 25$	$M = 64$
MADDPG	\$1.12	\$2.23	\$2.23	\$2.23
MFAC	\$1.12	\$2.23	\$2.23	\$2.23
EPC	\$6.12	\$6.12	\$6.12	\$9.18
DARL1N	\$1.08	\$1.84	\$2.81	\$7.02

Tab. 7: Hourly price rate for training each method in the Food Collection environment.

Method	Hourly Price Rate			
	$M = 3$	$M = 6$	$M = 12$	$M = 24$
MADDPG	\$1.12	\$1.12	\$2.23	\$2.23
MFAC	\$1.12	\$1.12	\$2.23	\$2.23
EPC	\$6.12	\$6.12	\$6.12	\$6.12
DARL1N	\$0.43	\$0.76	\$1.40	\$2.70

Tab. 8: Hourly price rate for training each method in the Grassland and Adversarial Battle environments.

Method	Hourly Price Rate			
	$M = 6$	$M = 12$	$M = 24$	$M = 48$
MADDPG	\$1.12	\$1.12	\$2.23	\$2.23
MFAC	\$1.12	\$1.12	\$2.23	\$2.23
EPC	\$6.12	\$6.12	\$6.12	\$9.18
DARL1N	\$0.43	\$0.76	\$1.40	\$2.70

From these results, we can make the following observations. In the Ising Model, when the number of agents is small (see Fig. 10(a)), DARL1N, MADDPG and MFAC spent roughly the same amount of money to converge, while EPC spent much more money to converge than the other methods. As the number of agents increases, the money spent by DARL1N becomes much less than that by MADDPG and MFAC. EPC spent the least amount of money, due to the use of curriculum learning. However, without curriculum learning, EPC spent

much more money than DARL1N to converge. In the Food Collection, Grassland, and Adversarial Battle environments as shown in Figs. 10(b), 10(c), 10(d), the amount of money spent for training DARL1N till convergence is similar as that spent for training MADDPG and MFAC, when the number of agents is relatively small. Nevertheless, when there are a large number of agents, DARL1N spent much less money to converge than the EPC. Although DARL1N spent roughly the same or slightly more money than MADDPG and MFAC for convergence, the convergence reward achieved by DARL1N is much higher than that of MADDPG and MFAC.

Visualization of Trained Agents To further demonstrate the quality of the policies learned by each method, we visualize the trained agents when playing different games in large-scale multi-agent settings, which are shown in Figs. 11-14.

Fig. 11 illustrates the states of the agents (spins) at the end of an episode in the Ising Model when there are $M = 64$ agents. Each grid represents an agent and the color of the grid indicates the value of the agent's state. Particularly, agents with states equal to -1 are marked in white and those with states equal to $+1$ are marked in black. As we can see, agents trained by EPC (see Fig. 11) can reach homogeneous states, and achieve the highest total reward. However, agents trained by the other methods are unable to reach homogeneous states.

States of a subset of agents at the end of an episode trained by different methods in the Food Collection environment when $M = 24$ are shown Fig. 12. As we can see, both EPC and DARL1N agents can reach food locations. However, agents learned by MADDPG and MFAC fail to reach any of the food locations.

Fig. 13 shows the states of a subset of agents during an episode in the Grassland environment when $M = 48$. We can observe that the good agents learned by EPC or DARL1N can successfully collect grass pellets. However, MADDPG and MFAC agents fail to do so. Moreover, the good agents learned by any of the four methods can be killed by the adversary agents.

Fig. 14 shows the states of a subset of agents during an episode in the Adversarial Battle environment when $M = 48$. It can be observed that both DARL1N and EPC agents can successfully collect resource units and kill agents from the other team, but MADDPG and MFAC fail to do so.

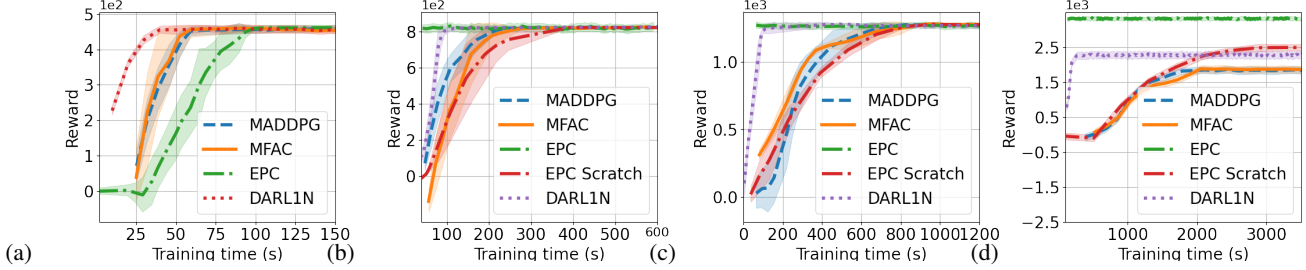


Fig. 6: Total training reward of different methods in the Ising model when there are (a) $M = 9$, (b) $M = 16$, (c) $M = 25$, and (d) $M = 64$ agents.

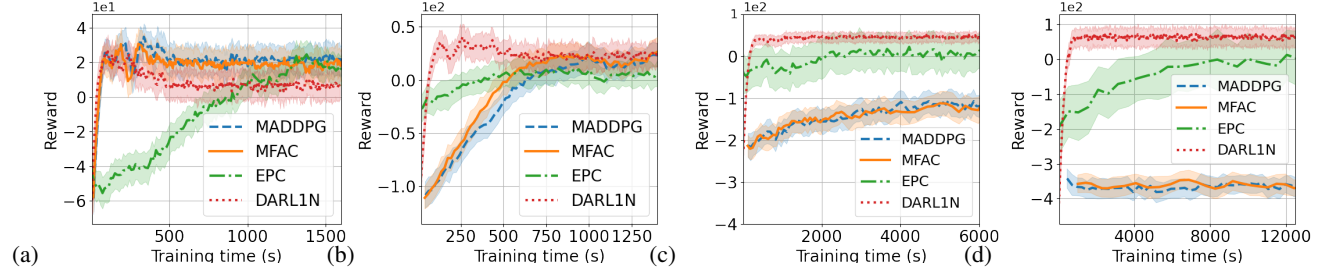


Fig. 7: Total training reward of different methods in the Food Collection environment when there are (a) $M = 3$, (b) $M = 6$, (c) $M = 12$, and (d) $M = 24$ agents.

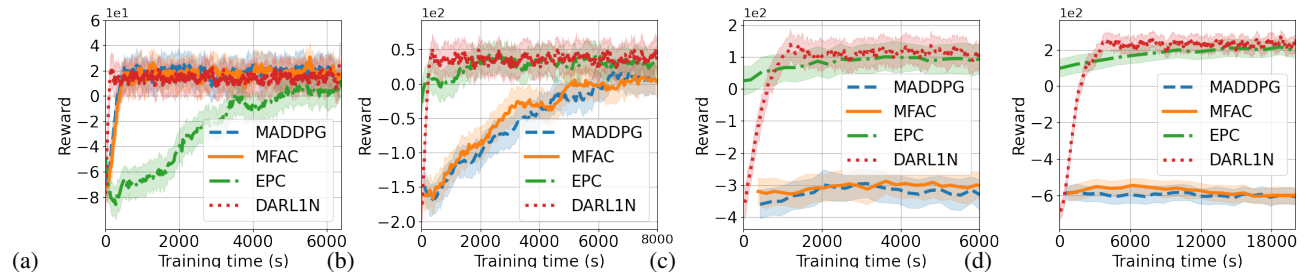


Fig. 8: Total training reward of good agents of different methods in the Grassland environment when there are (a) $M = 6$, (b) $M = 12$, (c) $M = 24$, and (d) $M = 48$ agents.

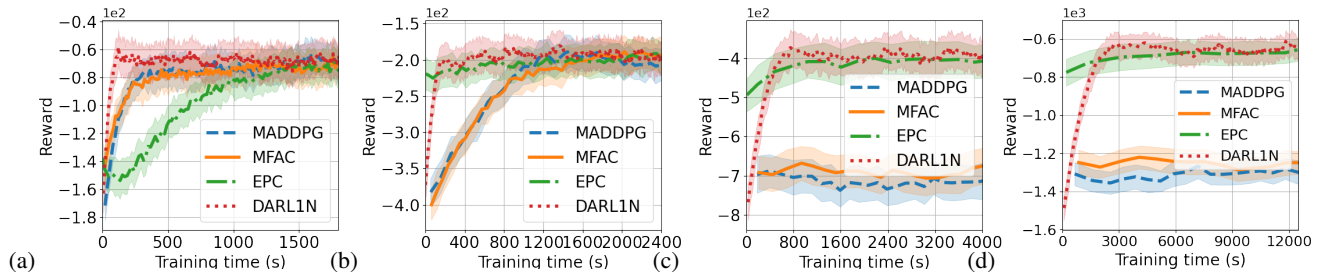


Fig. 9: Total training reward of good agents of different methods in the Adversarial Battle environment when there are (a) $M = 6$, (b) $M = 12$, (c) $M = 24$, and (d) $M = 48$ agents.

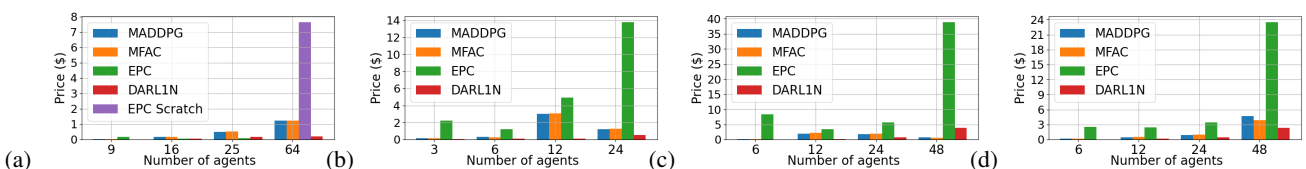


Fig. 10: Money spent for different methods to converge in the (a) Ising Model, (b) Food Collection, (c) Grassland and d) Adversarial Battle environments with different number of agents.

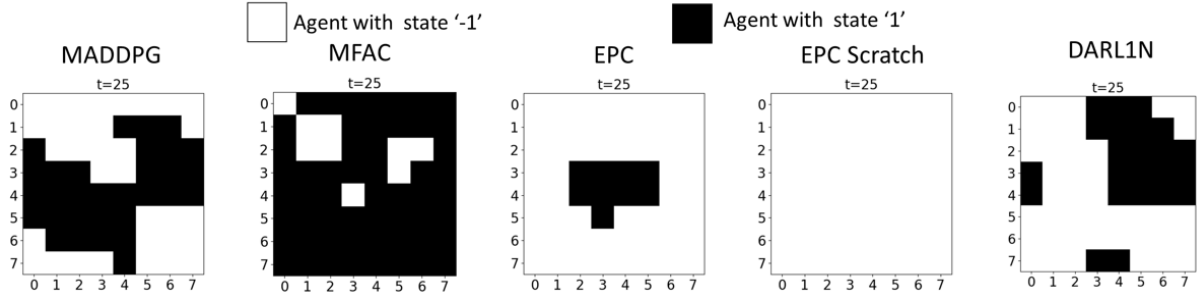


Fig. 11: States of the agents (spins) at the end of an episode in the Ising Model with agents trained by different methods when there are $M = 64$ agents.

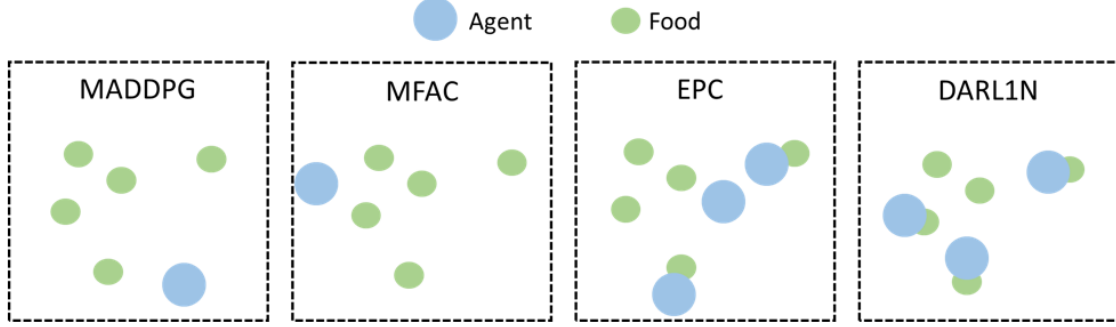


Fig. 12: States of a subset of agents at the end of an episode in Food Collection with agents trained by different methods when there are $M = 24$ agents.

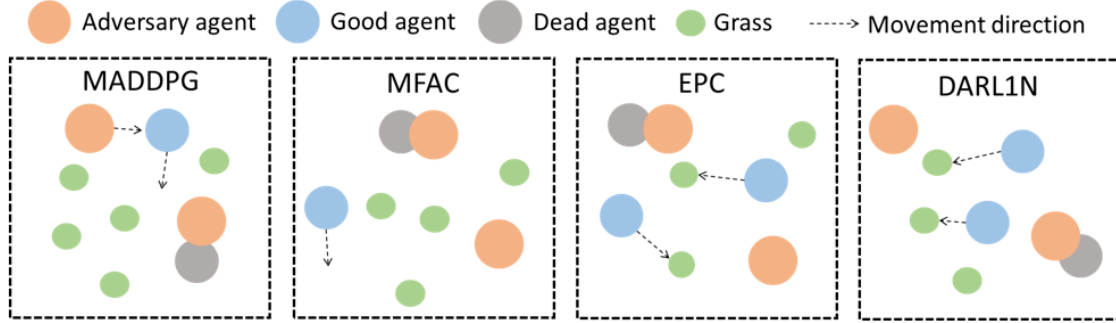


Fig. 13: States of a subset of agents during an episode in Grassland with agents trained by different methods when there are $M = 48$ agents.

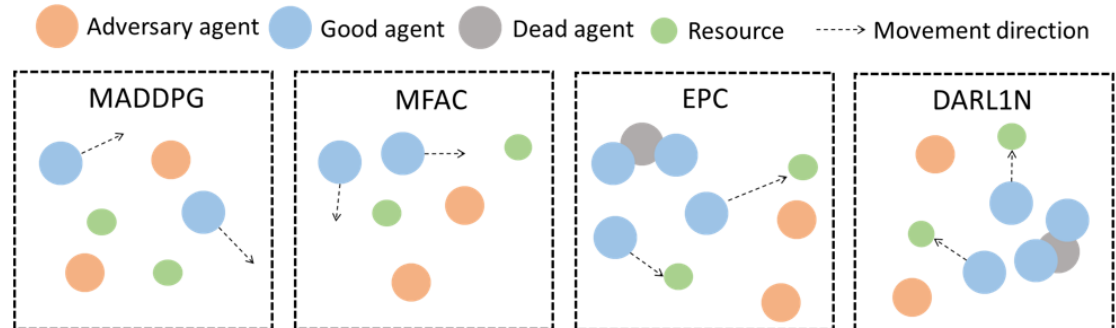


Fig. 14: States of a subset of agents during an episode in Adversarial Battle with agents trained by different methods when there are $M = 48$ agents.